

# A Molecular Dynamics Study on Au

Yasemin Öztekin Çiftci<sup>1</sup>, Kemal Çolakoğlu<sup>1</sup> and Soner Özgen<sup>2</sup>

<sup>1</sup>*Gazi University; Science Faculty, Physics Department, Ankara*

<sup>2</sup>*Firat University; Faculty of Art and Science, Physics Department, Elazığ  
Turkey*

## 1. Introduction

Theoretical and computational modeling is becoming increasingly important in the development of advanced high performance materials for industrial applications.[1] Computer simulations on various metallic systems usually use simple pairwise potentials. However, the interactions in real metallic materials can not be represented by simple pairwise interactions only. A pure pairwise potential model gives the Cauchy relation,  $C_{12}=C_{44}$ , between the elastic constants, which is not the case in real metals. Therefore, many-body interactions should be taken into account in any studies of metals and metal alloys.

It is very important to calculate the phase diagrams of metallic systems and their alloys in order to achieve technological improvements. The phase diagrams are still obtained by using experimental techniques because there are no available methods for entirely theoretical predictions of all of the phase diagrams of any pure metal. Therefore, in the calculations of the phase diagrams some expressions have been formed by using theoretical or semi-empirical approach and their validity have been investigated in a selected portion of the phase diagrams. The expressions suggested in semi-empirical approaches generally contain some factors depending on temperature and pressure. Therefore, the calculated phase region is restricted by experimental limits. Today, the free energy concepts, such as Gibbs and Helmholtz, on the other hand, have been widely used to calculate the macroscopic phase diagrams [2, 3] in which thermodynamics parameters are dominant. In microscopic scale, their calculations require some vibrational properties which can be derived from elastic constants of the material. So, the correct calculations of the elastic constants are important as well as the calculations of phase diagrams.

MD simulations can be utilized to compute the thermodynamic parameters and the results of the external effects, such as temperature and pressure or stress acted on a physical system [4, 5]. In the MD simulations, the interatomic interactions are modeled with a suitable mathematical function, and its gradient gives the forces between atoms. Hence, Newton's equations of motion of the system are solved numerically and the system is forced to be in a state of minimum energy, an equilibrium point of its phase space. Although many properties of the system, such as enthalpy, cohesive energy and internal pressure, have been directly calculated in the MD simulations, the entropy which is required for the free energy calculations has not been directly obtained and it is possible to obtain it by some approaches involved harmonic and anharmonic assumptions. There are some investigations related to

these approaches: the calculation of the free energy between FCC and HCP structures [6, 7], the investigation of first order phase transition [8], the dependence of the phase diagram on the range of attractive intermolecular forces [9], the investigation of harmonic lattice dynamics and entropy calculations in metal and alloys [10], the calculation of the  $P$ - $T$  diagram of hafnium [11], etc. Recently, the  $P$ - $T$  diagrams for Ni and Al have been calculated by Gurler and Ozgen [12] by using the MD simulations based on the EAM technique [13].

The reliability of the results obtained from MD simulations depends on the suitable modeling of the interatomic interactions. Interatomic interactions are usually results of fits to various experimental data. However, it is not clear whether simulations performed at other temperatures still reproduce the experimental data accurately. Comparing theoretical and experimental elastic constants and other properties at various temperatures can serve as a measure of reliability and usefulness of potential models [14, 15]. In fact, there are several potential energy functions that can be used for the metallic systems. However, the EAM, originally developed by Daw and Baskes [16, 17] to model the interatomic interactions of face-centered cubic (FCC) metals, has been successfully used to compute the properties of metallic systems such as bulk, surface and interface problems. The reliability of the EAM in the bulk and its simple form for use in computer simulations make it attractive.

When a liquid metal is quenched through the super-cooled region, a phase transition from liquid to glass takes place. Several techniques have been proposed to obtain a disordered state [18-20]. Among them the rapid solidification method is widely used for the amorphous phase. However, due to the demand of a high cooling rate this method is restricted in most experimental cases. Thus, the computer simulation of molecular dynamics is applied.

In this study, in order to model Au metallic systems we have used the EAM functions modified by us (Ciftci and Colakoğlu [21]), developed firstly by Cai [22]. In this work, we have carried out MD simulations to obtain the  $P$ - $V$  diagrams at 300 K and the  $P$ - $T$  diagrams of the systems for an ideal FCC lattice with 1372 atoms, by using an anisotropic MD scheme. In addition, the bulk modulus and specific heat of the system in solid phase are determined and results-driven simulations are interpreted by comparing with the values in literature. We have also calculated the pressure derivatives of elastic constants and bulk moduli for Au. The obtained results are compared with the values in the literature. The another purpose of this work is to explore the glass transition and crystallization of Au using EAM .

## 2. Potential energy function

According to the embedded atom method, the cohesive energy of an assembly of  $N$  atoms is given by [16, 17]

$$E_{tot} = \sum_i F_i(\rho_i) + \sum_{i>j} \phi(r_{ij}) \quad (1)$$

$$\rho_i = \sum_{j(\neq i)} f(r_{ij}), \quad (2)$$

where  $E_{tot}$  is the total cohesive energy,  $\rho_i$  is the host electron density at the location of atom  $i$  due to all other atoms,  $f(r_{ij})$  is the electronic density function of an atom,  $r_{ij}$  is the distance

between  $i$  and  $j$  atoms,  $F_i(\rho_i)$  is the embedding energy to embed atom  $i$  in an electron density  $\rho_i$ , and  $\phi(r_{ij})$  is the pairwise potential energy function between atoms  $i$  and  $j$ .

In this work, we used a modified pairwise potential function in the framework of the Cai version [22] of the EAM. Recently, this potential function has been used by us for predicting several physical properties of some transitional metals [21,23-25]. The present form of the potential makes it more flexible owing to the constants,  $m$  and  $n$  in the multiplier forms. Such a factor included in the classical Morse function is treated by Verma and Rathore [26] to compute the phonon frequencies of Th, based on the central pair potential model. The modified parts of the potential and the other terms are as follows:

$$f(r) = f_e e^{-\alpha(r-r_e)}, \quad (3)$$

$$F(\rho) = -F_0 \left[ 1 - \ln \left( \frac{\rho}{\rho_e} \right) \right]^n \left( \frac{\rho}{\rho_e} \right)^n + D_2 \left( \frac{\rho}{\rho_e} \right), \quad (4)$$

$$\phi(r) = \frac{D_1}{(m-1)} \left[ \frac{e^{-m\beta\left(\frac{r}{r_e}-1\right)}}{\left(\beta\frac{r}{r_e}\right)^n} - \left(\beta\frac{r}{r_e}\right)^n e^{-\beta\left(\frac{r}{r_e}-1\right)} \right], \quad (5)$$

where  $a$ ,  $\beta$ ,  $D_1$  and  $D_2$  are fitting parameters that are determined by the lattice parameter  $a_0$ , the cohesive energy  $E_c$ , the vacancy formation energy  $E_v^f$ , the elastic constants  $C_{ij}$ . Here  $\rho_e$  is the host electron density at equilibrium state,  $r_e$  is the nearest neighbor equilibrium distance, and  $F_0 = E_c - E_v^f$ . In this potential model, there are four parameters:  $\beta$  and  $D_1$  are from two-body term,  $m$  and  $n$  are adjustable selected constants. The fitting parameters are determined by minimizing the value of  $W = \sum [(X^{cal} - X^{exp}) / X^{exp}]^2$ . Here  $X$  represents the calculated and experimental values of the quantities taken into account in the fitting process. Hence, the potential functions can be fitted very well to the experimental properties of the matter, such as the vacancy formation energy ( $E_v$ ), cohesive energy ( $E_c$ ), elastic constants ( $C_{ij}$ ), and lattice constants ( $a_0$ ) in an equilibrium state. In the fitting process here, the cutoff distance is taken to be  $r_{cut} = 1.65a_0$ . In the Eq. (3), the  $f_e$  parameter is selected as unity for mono atomic systems because it is used for alloy modeling as an adjustable parameter to constitute suitable electron density. For the selected values of the constants  $m$  and  $n$ , the computed potential parameters and experimental input data for Au are given in Table 1.

The cohesive energy changes with the variation of lattice constants of Au calculated from Eq. (1) and from the general expression of the cohesive energy of metals proposed by Rose et al. [32] are compared in Fig.1. The Rose energy is also called as the generalized equation of state of metals and written as

$$E_R(a^*) = -E_0(1 + a^*)e^{-a^*} \quad (6)$$

$$a^* = \left( \frac{a}{a_0} - 1 \right) / \left( \frac{E_c}{9B_m \Omega} \right)^{1/2} \quad (7)$$

where  $E_0$  is a constant to be taken as an equilibrium cohesive energy of solid,  $B_m$  is the bulk modulus, and  $\Omega$  is the atomic volume in equilibrium. It has been determined that the cohesive energy calculated from Eq. (1) with the parameter given in Table1 for Au is in good agreement with Rose energies in equilibrium.

	$a_0$	$r_0$	$E_c$	$E_v^f$	$B_m$	$C_{11}$	$C_{12}$	$C_{44}$	$T_m$	$C_p$
	(Å)	(Å)	(eV)	(eV)	(GPa)	(GPa)	(Gpa)	(GPa)	(K)	(K/mol.K)
Au	4.079	2.8842	3.81	0.93	180.32	201.63	169.67	45.44	1337	25.42

	$m$	$n$	$\alpha$	$\beta$	$D_1$	$D_2$
			(Å <sup>-1</sup> )		(eV)	(eV)
Au	7	0.5	4.3482	3.5361	0.0685	0.3097

Table 1. The experimental properties and potential parameters of Au. The experimental lattice parameters ( $a_0$ ) at room temperature are from ref. [27]. Bulk modulus ( $B_m$ ) and elastic constants ( $C_{ij}$ ) given at zero temperature are from [28], vacancy formation energy ( $E_v^f$ ) is from ref. [29], melting temperature ( $T_m$ ), the coefficient of linear thermal expansion  $\alpha$  are from [30], and specific heat  $C_p$  is from [31].

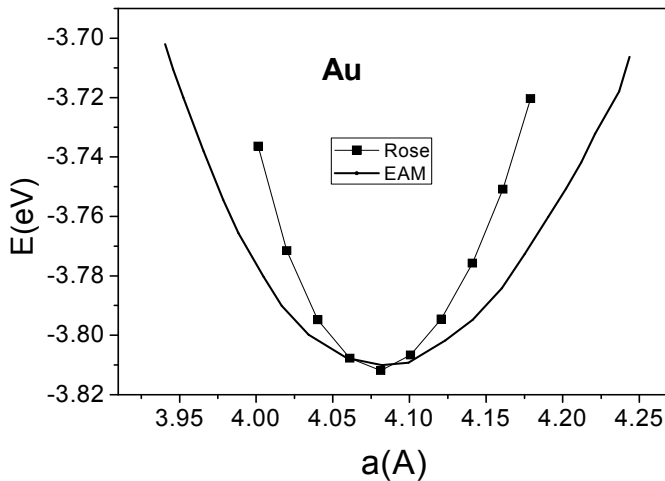


Fig. 1. Rose and EAM energies versus lattice constant for Au.

### 3. Molecular dynamics simulation

The Lagrange function, written for an anisotropic box, i.e. MD cell, containing  $N$  particles by Parrinello and Rahman, is given by [33, 34]

$$L_{PR} = \frac{1}{2} \sum_{i=1}^N m_i (\dot{\mathbf{s}}_i^t \mathbf{G} \dot{\mathbf{s}}_i) - E_{tot} + \frac{1}{2} M \text{Tr}(\dot{\mathbf{h}}^t \dot{\mathbf{h}}) - P_{ext} V, \tag{8}$$

where  $m_i$  is mass of particle  $i$ ,  $\mathbf{s}_i$  is the scaled coordinate of atom  $i$  and is represented by a column vector whose elements are between zero and unity,  $\mathbf{h}=(\mathbf{a}, \mathbf{b}, \mathbf{c})$ ;  $\mathbf{a}$ ,  $\mathbf{b}$  and  $\mathbf{c}$  vectors are MD cell axes, the metric tensor  $\mathbf{G}$  is given by matrix product  $\mathbf{h}^t\mathbf{h}$ ,  $M$  is an arbitrary constant which represents mass of the computational box,  $P_{\text{ext}}$  is external pressure applied on the cell,  $V$  is the volume of the MD cell and is obtained from  $\det(\mathbf{h})$ . Thus, square of distance between particles  $i$  and  $j$  is described by  $r_{ij}^2 = s_{ij}^t G s_{ij}$ . The classical equations of motion of the system obtained from Eq. (1) become

$$\ddot{\mathbf{s}}_i = -\frac{1}{m_i} \mathbf{F}_i = \mathbf{G}^{-1} \hat{\mathbf{G}} \dot{\mathbf{s}}_i \quad (9)$$

$$\ddot{\mathbf{h}} = M^{-1} (\mathbf{\Pi} - \mathbf{I} P_{\text{ext}}) \boldsymbol{\sigma} \quad (10)$$

where  $\boldsymbol{\sigma} = (\mathbf{bxc}, \mathbf{cxa}, \mathbf{axb}) = V(\mathbf{h}^t)^{-1}$  and microscopic stress tensor,  $\mathbf{\Pi}$ , is a dyadic given as follows;

$$\mathbf{\Pi} = V^{-1} \left[ \sum_{i=1}^N m_i \mathbf{v}_i \cdot \mathbf{v}_i - \sum_{i=1}^N \sum_{j>i}^N \frac{F_{ij}}{r_{ij}} \mathbf{r}_i \cdot \mathbf{r}_i \right] \quad (11)$$

Also the force on an atom  $i$  in the system is calculated from the following equation,

$$\mathbf{F}_i = -\Delta_s E_i = -\sum_{\substack{j=1 \\ j \neq i}}^N \left[ F'_i \rho'_j + F'_j \rho'_i + \phi'_{ij} \right] \frac{\hat{\mathbf{s}}_{ij}}{r_{ij}} \quad (12)$$

where the primes denote the first derivatives of the functions with respect to their arguments.

In all of the simulation studies, the equation of motion given in Eqs. (9) and (10) were numerically solved by using the velocity version of the Verlet algorithm [35]. The size of integration step was chosen to be  $7.87 \times 10^{-15}$ s for Au. Initial structures of the systems were constructed on a lattice with 1372 atoms and an FCC unit cell. It has been observed that, with these initial conditions, the systems were equilibrated in 5000 integration steps. Time averages of the thermodynamic properties of the system in each simulation run were determined by using 30,000 integration steps following the equilibration of the system. The structures of the system in solid phase were examined by using the radial distribution function. Melting temperatures were determined from the plots of the cohesive energy versus temperature. It is possible to classify our simulation runs in two groups as thermal and pressure applications. In the thermal applications, the temperature of the system under zero pressure is raised from 100K to 2400K for Au with an increment of 100K in each run of 35,000 integration step; but near the melting temperatures, the increment is reduced to 20K. The pressure applications are also implemented by repeating the thermal applications under pressure values of 0.5, 1.0, 1.5, 2.5, 5.0, 7.5, 10.0, 15.0 and 20.0 GPa. The simulation is restarted with different pressure in each run, to avoid algorithmic errors.

The temperature dependency of the elastic constants and the bulk moduli are calculated by following the procedure given by Karimi et al [14].

For the calculation of glass formation and crystallization, firstly, we run 20 000 time steps to make the system into equilibrium state, then the liquid phase is cooled to 100K at the rate of  $1.5833 \times 10^{13}$  K/s and  $1.5833 \times 10^{12}$  K/s, respectively to examine the formation process of amorphization and crystallization.

## 4. Results and discussion

### 4.1 Thermal and mechanical properties

We can classify our results on thermal and mechanical properties of Au in to seven different categories (i) the  $P$ - $V$  diagram has been analyzed to determine the bulk modulus under zero pressure, (ii) the specific heat has been determined by using the changes of the enthalpy with temperature, (iii) the radial distribution function has been obtained in solid and liquid phases for the estimation of structural properties, (iv) the  $P$ - $T$  graph, which is plotted by using the variation in melting temperatures with increasing pressure acted on the system, have been examined. (v) the pressure dependence of  $V/V_0$  has been obtained, (vi) elastic constants and pressure derivatives of elastic constants and bulk modulus has been investigated.

The change on the atomic volume with the gradually increasing pressure, which acts on the system at 300K temperature, is given in Fig.2 for Au. The bulk modulus calculated from the  $P$ - $V$  diagram shown in Fig.2 is obtained as  $B=174.3$  GPa for Au. The calculated bulk modulus is in good agreement with their experimental values (see Table 1) within an error of  $\sim 3.4\%$  for Au.

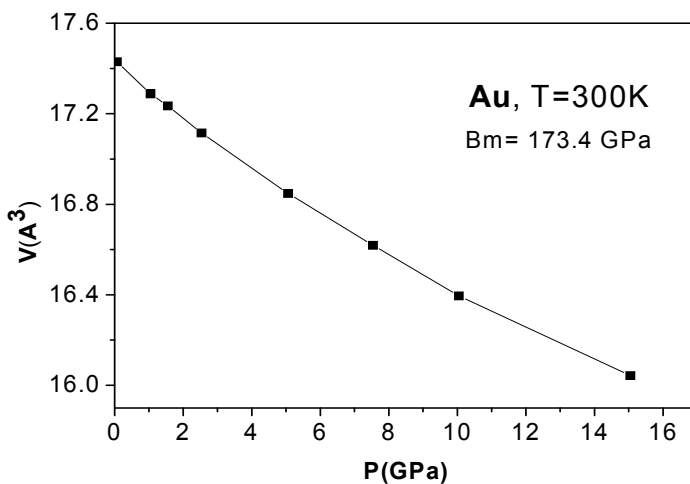


Fig. 2.  $P$ - $V$  diagrams for Au.

The variations of enthalpy with temperatures under zero pressure for solid Au is given in Fig.3, and this graph is used to compute specific heats under the constant pressure. The calculated values of specific heats over 0-300K are found to be  $C_p = 28.2$  J/molK for Au.

Considering the experimental data in Table 1, it can be seen that the specific heat is calculated with an error of 9.8 % for Au.

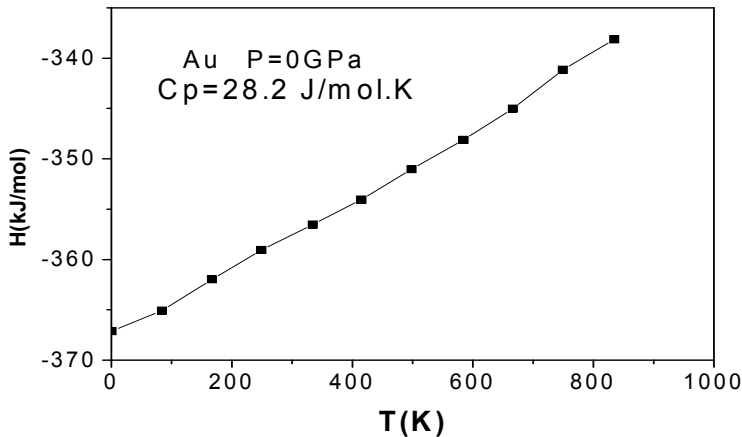


Fig. 3. Variation of the enthalpy with temperature for Au.

There are several methods for determining the melting temperature of a crystal. MD simulations are performed on system at various temperatures, and the cohesive energy is plotted as a function of temperature in one of these methods, as we did here. At the melting point, a discontinuity occurs in the cohesive energy. The other way of determining the melting temperature is to plot caloric curve which is the change of the total energy of crystal versus kinetic energy [36]. Indeed, the melting temperature of metal is obtained as the temperature at which the Gibbs free energy of the solid and liquid phases become equal. The entropy is required to compute the free energy, but it can not be directly calculated from MD simulations. For this reason, some other approaches are required [3]. Another way of determining the melting temperature is to simulate the solid-liquid interface [14]. In this way, the temperature for which the interface velocity goes to zero is determined as the melting temperature and it is reproduced more correctly than the way of caloric curve. Karimi et al [14] estimated the melting temperature for Ni as  $1630 \pm 50$  K within an error of -5.6%, using the solid-liquid interface technique.

In the present work, the variations of cohesive energy with temperature for different pressures acted on the system are given in Fig. 4 for Au. We have computed the melting temperatures under zero pressure as  $1100 \pm 20$  K for Au. When these values are compared with the experimental ones of 1337 K given in Table 1, the error for Au becomes 21%.

The radial distribution function (RDF) is used to investigate the structural properties of the solid and liquid phases. The plot of radial distribution functions acquired in solid and liquid phases for Au is given in Fig. 5. First peak location of radial distribution curves represents the distance of the nearest neighbor atoms,  $r_0$ . The second peak location denotes the distances of next nearest neighbors,  $a_0$ . These distances are found to be  $2.907 \text{ \AA}$  and  $4.144 \text{ \AA}$ , respectively for Au. By comparing with experimental data given in Table 1, the calculated

error on  $a_0$  and  $r_0$  are 0.8% and 1.5% for Au. So, the present errors can be omitted since the parameters of the potential energy function were fitted to the crystal properties in static case. Since the peak locations shown in Fig. 5 satisfy the certain peak locations at  $\sqrt{2}$ ,  $\sqrt{3}$ ,  $\sqrt{4}$ ,  $\sqrt{5}$ , etc. times  $r_0$  in an ideal FCC unit cell, the metal of Au has an FCC unit cell under zero pressure.

The  $P$ - $T$  diagrams plotted by using the melting temperatures under different pressures are given in Fig. 6 for Au. The binding energies of the metals can be reduced by increasing temperature. At high temperatures near the melting point, it is generally expected that the Gibbs free energy is lowered by phase transition like martensitic types from one structure to another one which has lower energy at higher temperatures, like a BCC lattice.

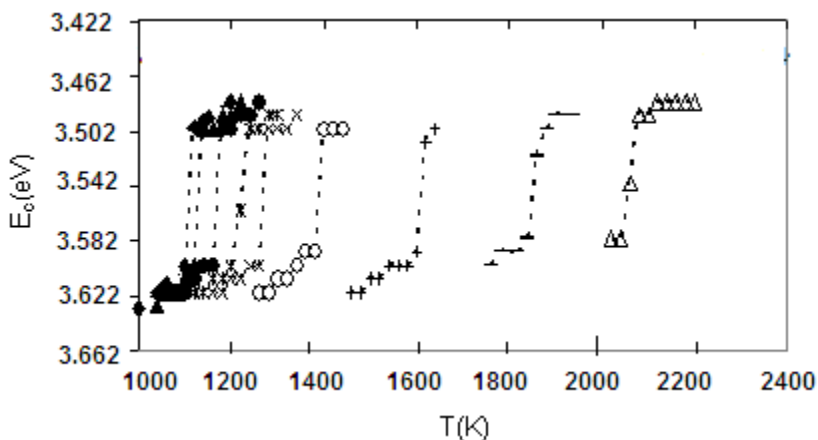


Fig. 4. The cohesive energy as a function of temperature at different pressure for Au. The symbols  $\blacklozenge, \blacktriangle, \bullet, \times, \ast, \circ, +$  represents the pressure values of 0.0, 0.5, 1.0, 1.5, 2.5, 5.0, 7.5 GPa, respectively.

We calculated  $V/V_0$  as a function of pressure (0-45 kbar) for Au and added experimental points [37] for comparing with MD results. The plot of  $V/V_0$  versus pressure for Au is given in Fig. 7. Here  $V_0$  is the volume under the zero pressure. MD results are in very good agreement with the experimental data at pressures below 25GPa.

We also calculated elastic constants and pressure derivatives of the elastic constants and bulk modulus at 0 K and in  $P=0$  GPa pressure. The results are summarized in Table 2. Obtained results are in good agreement with available other theoretical results.

	$C_{11}$ (GPa)	$C_{12}$ (GPa)	$C_{44}$ (GPa)	$(\partial C_{11}/\partial P)_T$	$(\partial C_{12}/\partial P)_T$	$(\partial C_{44}/\partial P)_T$	$(\partial B/\partial P)_T$
This study	195.43	163.67	44.56	6.99	3.98	2.01	4.02
[38]	192.9	162.8	41.5	5.72	4.96	1.52	4.66
[39]	192.2	162.8	42.0	7.01	6.14	1.79	6.43

Table 2. Second order elastic constants and pressure derivatives of elastic constants and bulk modulus ( $P=0$  GPa).

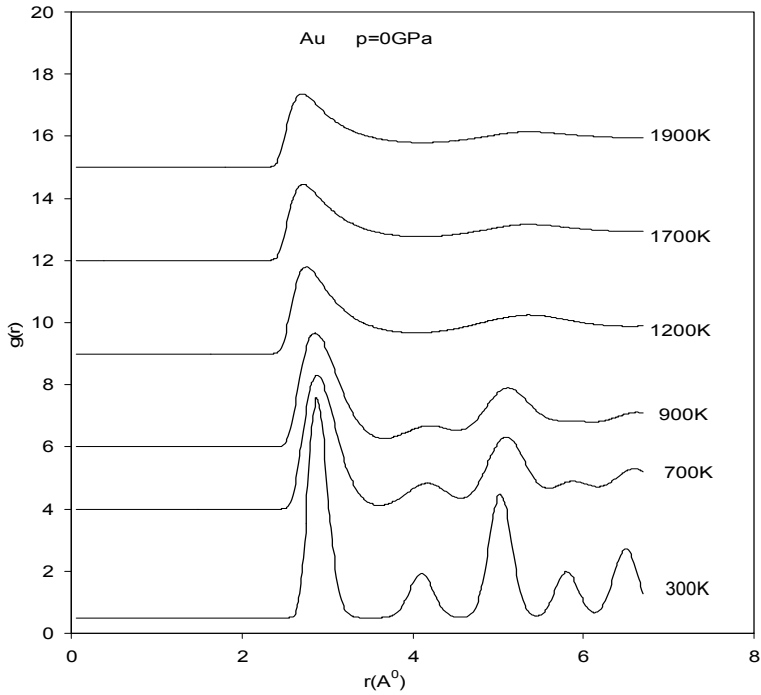


Fig. 5. The radial distribution curves in solid and liquid phases for Au.

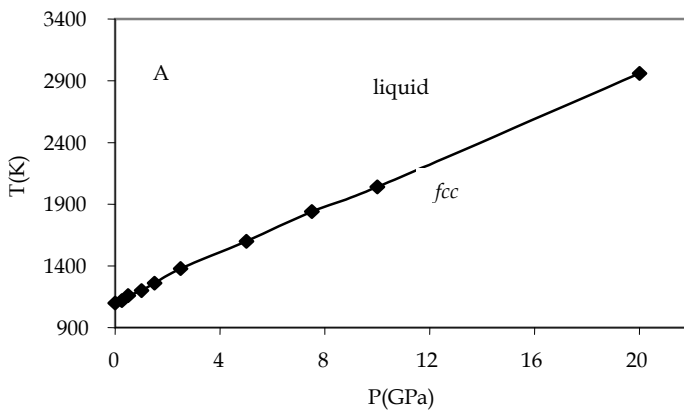


Fig. 6. P-T diagrams for Au.

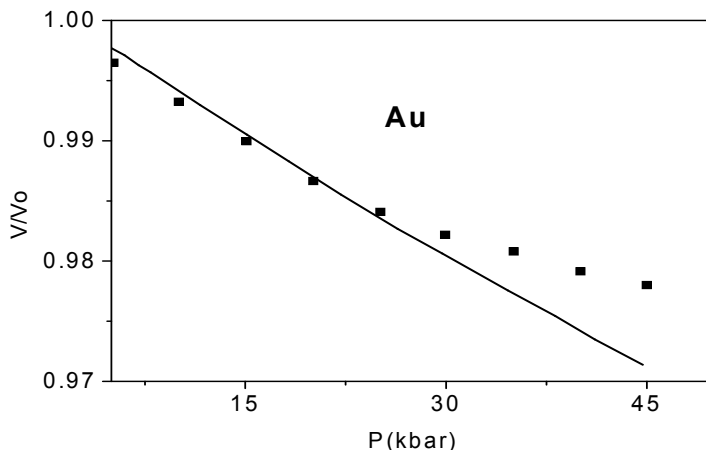


Fig. 7. Variation of pressure as a function of  $V/V_o$  for Au. Experimental points are taken from Ref.[37].

#### 4.2 Glass formation and crystallization

Traditionally, the heating and cooling processes are applied to examine the formation process of amorphization and crystallization. The Fig.8(a) and (b) show the variation of volume at the rate of  $1.5833 \times 10^{13}$  K/s and  $1.5833 \times 10^{12}$  K/s, respectively. The sudden jump in volume in the temperature range of 1000 to 1100K for the heating process is due to the melting of the Au. In contrast to heating, cooling curves show a continuous change in volume.

The slope of the volume versus temperature curve in Fig.8(a) at the rate of  $1.5833 \times 10^{13}$  K/s decreases below 500K. This is a sign of glass formation. Since the glass is a frozen liquid, the change in configurational entropy vanishes. Thus, the derivative of entropy with respect to pressure is the derivative of volume with respect to temperature[40]. The Fig. 8(b) at rate of  $1.5833 \times 10^{12}$  K/s shows a sharp change in the volume as the temperature is lowered below 300K. At 350 K system shows that the cooled Au has crystallized.

Different methods are suggested to determine the glass transition temperature ( $T_g$ ) which is observed widely in amorphous materials. According to one of these definitions, which is known as Wendt-Abraham ratio [41], to determine  $T_g$  in MD simulations, the  $g_{min}/g_{max}$  ratios of RDF curves at different temperatures are calculated [39]. Here,  $g_{min}$  is the first minimum value and  $g_{max}$  is first maximum value of RDF curve. In such a plot, two lines in different slopes occur, and glass transition temperature is taken as intersection point of these lines. The graph of  $g_{min}/g_{max}$  ratios versus temperature obtained in this study is given in Fig. 9. The  $T_g$  is obtained from this figure to be 500K.

The RDF curves of the model structure during the heating and cooling processes at different temperature are given in Fig10. The RDF shows an fcc crystal structure as the sample is heated from 0 to 500 K. But, at 1200 K (above the melting temperature) the emergence of

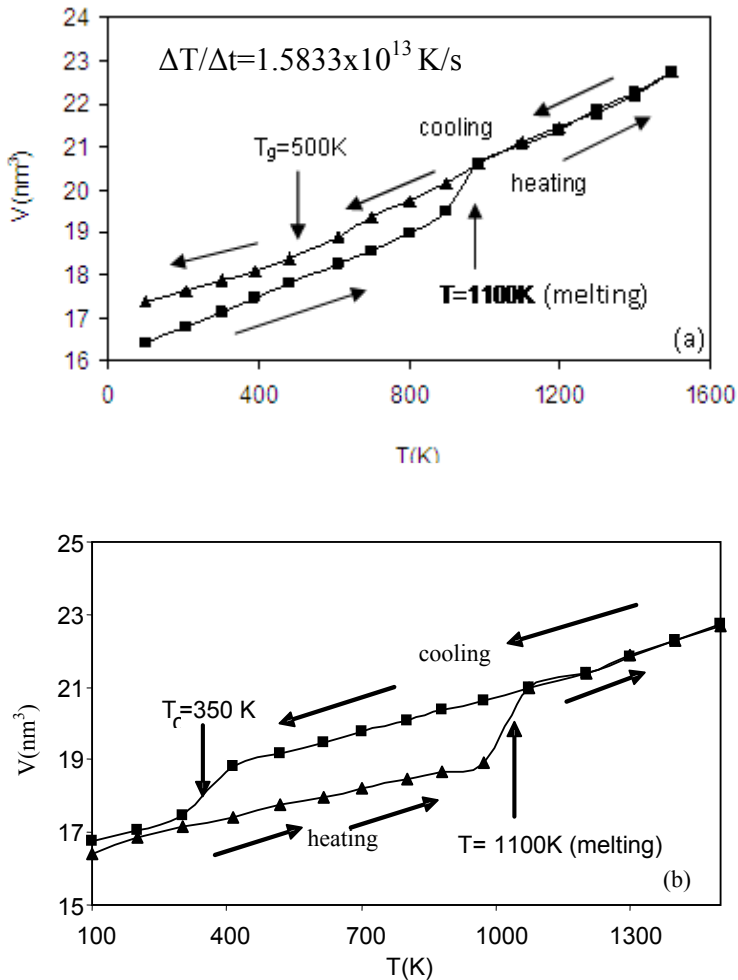


Fig. 8. Average volume of Au during heating and cooling at a rate of (a)  $1.5833 \times 10^{13} \text{ K/s}$  and (b)  $1.5833 \times 10^{12} \text{ K/s}$ .

broad peaks shows that the structure has melted. The sample was heated to 1500K and then cooled back to 1200 K, leading to the same structure as for heating, indicating a stable liquid state. Cooling to 500K, from RDF we still see the structure of a liquid, in fact a supercooled liquid. However, after cooling to 300K, we see that the second peak of RDF is split. This splitting of the second peak is a well-known characteristic feature in the RDF of a metallic glass.

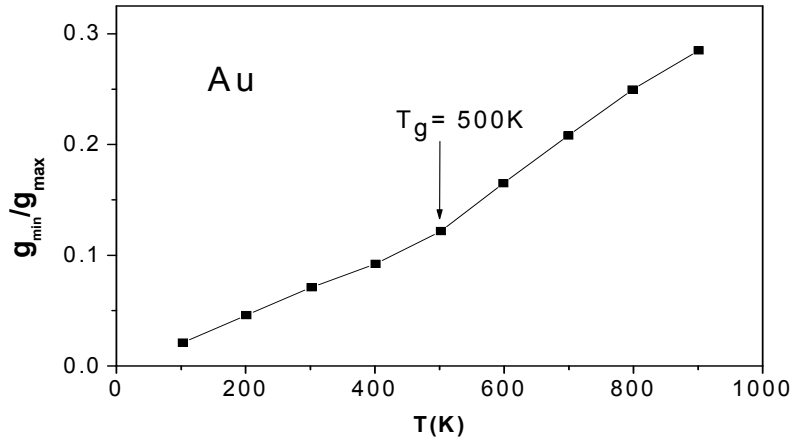
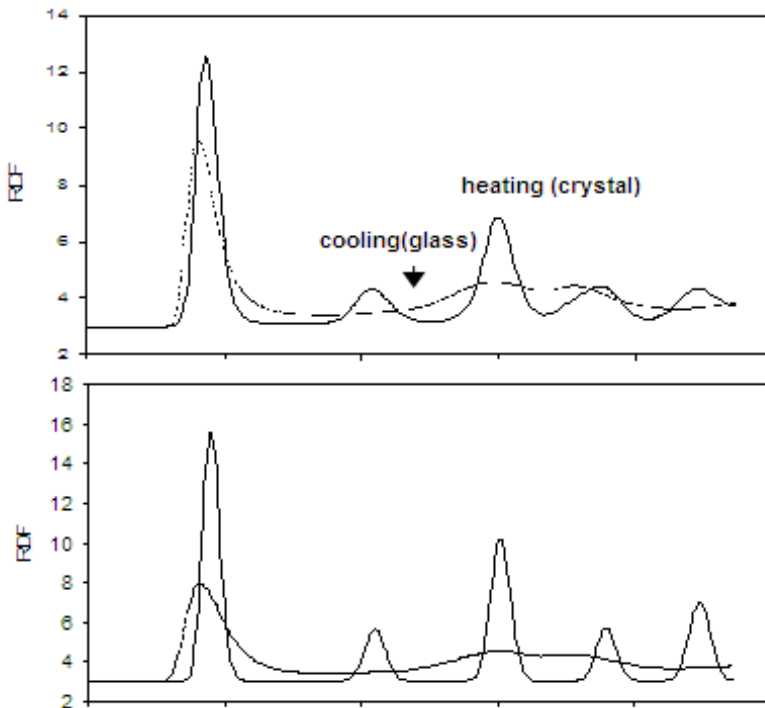


Fig. 9. Determination of glassy transition temperature.



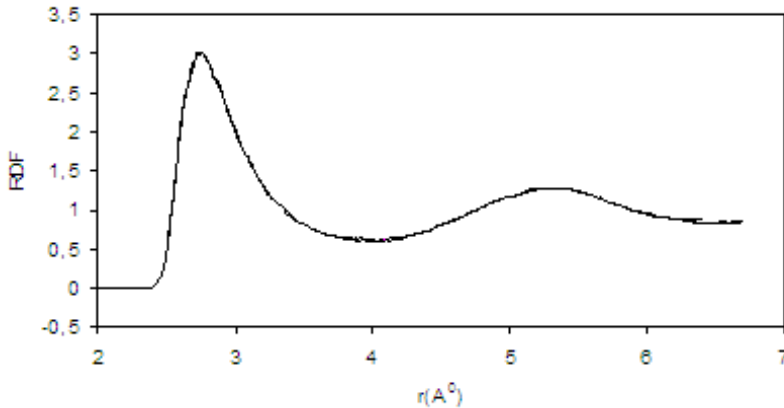


Fig. 10. Radial distribution function (RDF) of Au during the heating and cooling processes at rate of  $1.5833 \times 10^{13}$  K/s (a) at 0K (b) at 500 K, and (c) at 1200K.

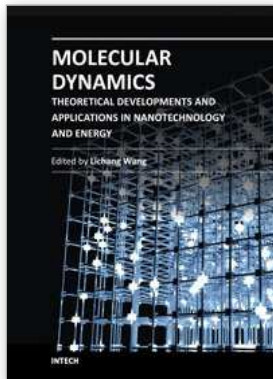
## 5. Conclusion

It has been found that the present version of EAM with a recently developed potential function, which makes it more flexible owing to the parameter  $n$ , represents quite well the interactions between the atoms to simulate the studied mono atomic systems. Since the parameterization technique of our potential is based on the bulk properties of metals at 0K, it can describe the temperature-dependent behaviors of our crystals particularly, qualitatively. As a whole, present model well describes the many physical properties, and our results are in reasonable agreement with the corresponding experimental findings, and provide another measure of the quantitative limitations of the EAM for bulk metals.

## 6. References

- [1] T. Çağın, G. Dereli, M. Uludoğan, and M. Tomak, Phys. Rev. B, 59,5, (1999)3468.
- [2] P. Haasen, Physical Metallurgy, 2 nd ed., Cambridge Univ. Press., UK, 1992.
- [3] D. A. Porter, K.E. Easterling, Phase Transformation in Metals and Alloys, 1, 2<sup>nd</sup> ed., Chapman& Hall, T. J. Press (Padstow), UK, 1992.
- [4] J.M. Haile, Molecular Dynamics Simulation, Elementary Methods, Wiley, Canada, 1992.
- [5] C.R.A Catlow., in: C.R.A Catlow. et al. (Eds.), Computer Modelling of Fluids Polymers and Solids, Kluwer Academic Publishing, USA, 1990, pp. 1-28.
- [6] M.C. Moody, J.R. Ray, J. Chem. Phys. 84 (3) (1986) 1795.
- [7] J. Ihm, Rep. Prog. Phys. 51 (1988) 105.
- [8] W.C. Kerr, A.M. Hawthorne, R.J Gooding, A.R Bishop., J. A Krumhansl, Phys. Rev. B 45 (13) (1992) 7036.
- [9] M. Hasegawa, K. Ohno, J. Phys. Condens. Matter, 9 (1997) 3361.
- [10] G.D. Barrera, R.H. Tendler, Comput. Phys. Commun.,105 (1997) 159.
- [11] S.A. Ostanin, V.Y. Trubitsin, Comput. Mater. Sci., 17 (2000) 174.

- [12] Y.Gurler, S. Ozgen, *Matt. Lett.* 57 (2003) 4336.
- [13] M. W. Finnis, J.E. Sinclair, *Philos. Mag.*, A. 50 (1) (1984) 45.
- [14] M. Karimi, G. Stapy, T. Kaplan and M. Mostoller, *Modelling Simul. Mater. Sci. Eng.*, 5 (1997) 337.
- [15] S. Erkoç, *Phys. Rep.* 278 (1997) 79.
- [16] M.S. Daw, M.I. Baskes, *Phys. Rev. Lett.*, 50 (17) (1983) 1285.
- [17] M.S. Daw, M.I. Baskes, *Phys. Rev. B*, 29(12) (1984) 6443.
- [18] C. Massobric, V. Pontikis, G. Martin, *Phys. Rev. B*, 41(15)(1990)10486.
- [19] F. Cardellini, V. Contini, G.Mazzone, *Scripta Metall Mater*, 4(1995) 641.
- [20] J.S.C. Jang, C.C. Koch, *J. Mater Res.*, 5(3)(1990) 498.
- [21] Y.O Ciftci. and K.Colakoglu, *Acta Physica Polonica A*, (100)4 (2001) 539.
- [22] J. Cai and Y.Y. Ye, *Phys. Rev.B* 54 (12) (1996) 8398.
- [23] S. Kazanc, Y.O. Ciftci, K.Colakoglu, and S.Ozgen, *Physica B*, 381(2006)96.
- [24] Y.O. Ciftci, K.Colakoglu, S.Ozgen and S.Kazanc, *Cent. Eur. J.Phys.* 4(2006)472.
- [25] Y.O. Ciftci, K.Colakoglu, S.Ozgen and S.Kazanc, *J. Phys: Condens. Matter* 19 (2007) 326204.
- [26] M.L. Verma, R.P.S. Rathore, *Phys. Stat. Sol. b*, 185 (1994) 93.
- [27] W. B.Pearson, *Handbook of lattice Spacing and structure of Metals and Alloys*, Pergamon, Oxford,1967.
- [28] R. O. Simmons and H. Wang, *Single Crystal Elastic Constants and Calculated Aggregate Properties,A Handbook*, MIT Press, Cambridge, 1991
- [29] *Londolt -Bornstein New Series*, vols. III-11 and III-18, Springer -Verlag, Berlin,1991
- [30] C. Kittel, *Introduction to solid state physics*, Wiley, New York,1986.
- [31] Y. S. Touloukian and E.H. Buyco, *Specific Heat: Metallic Elements and Alloys* (New York:IFI/ Plenum, 1970)
- [32] J. H. Rose, J.R Smith., F Guinea., J. Ferrante, *Phys. Rev. B.* 29(6) (1984) 2963.
- [33] M. Parrinello, A. Rahman, *Phys. Rev. Lett.* 45(11) (1980) 1196.
- [34] M. Parrinello, A. Rahman, *J. App. Phys.* 52 (12) (1981) 7182.
- [35] L. Verlet, *Phys. Rev.* 159 (1967) 98.
- [36] S.K. Nayak, S.N. Khanna, B.K. Rao, P. Jena, *J. Phys. Cond. Mat.*, 10 (1988) 10853.
- [37] M.H. Rice, R.G. McQueen , J.H. Walsh, *Solid State Physics*, 6 (1958) 1.
- [38] Y. Hiki, A.Granato, *Phys. Rev. B*, 144 (1966) 411.
- [39] W.B. Daniels, C.S. Smith, *Phys. Rev. B*, 111 (1958) 713.
- [40] Y. Qi, T. Çağın, Y. Kimura, and W.A. Goddard, *Phys. Rev. B*, 59(5) (1999)3527.
- [41] L.Wang, X.B. Fang, H. Li, *Mater. Lett.* 51(2001) 7.



## **Molecular Dynamics - Theoretical Developments and Applications in Nanotechnology and Energy**

Edited by Prof. Lichang Wang

ISBN 978-953-51-0443-8

Hard cover, 424 pages

**Publisher** InTech

**Published online** 05, April, 2012

**Published in print edition** April, 2012

Molecular Dynamics is a two-volume compendium of the ever-growing applications of molecular dynamics simulations to solve a wider range of scientific and engineering challenges. The contents illustrate the rapid progress on molecular dynamics simulations in many fields of science and technology, such as nanotechnology, energy research, and biology, due to the advances of new dynamics theories and the extraordinary power of today's computers. This first book begins with a general description of underlying theories of molecular dynamics simulations and provides extensive coverage of molecular dynamics simulations in nanotechnology and energy. Coverage of this book includes: Recent advances of molecular dynamics theory Formation and evolution of nanoparticles of up to 106 atoms Diffusion and dissociation of gas and liquid molecules on silicon, metal, or metal organic frameworks Conductivity of ionic species in solid oxides Ion solvation in liquid mixtures Nuclear structures

### **How to reference**

In order to correctly reference this scholarly work, feel free to copy and paste the following:

Yasemin Öztekin Çiftci, Kemal Çolakoğlu and Soner Özgen (2012). A Molecular Dynamics Study on Au, Molecular Dynamics - Theoretical Developments and Applications in Nanotechnology and Energy, Prof. Lichang Wang (Ed.), ISBN: 978-953-51-0443-8, InTech, Available from:  
<http://www.intechopen.com/books/molecular-dynamics-theoretical-developments-and-applications-in-nanotechnology-and-energy/a-molecular-dynamics-study-on-au>

**INTECH**  
open science | open minds

### **InTech Europe**

University Campus STeP Ri  
Slavka Krautzeka 83/A  
51000 Rijeka, Croatia  
Phone: +385 (51) 770 447  
Fax: +385 (51) 686 166  
[www.intechopen.com](http://www.intechopen.com)

### **InTech China**

Unit 405, Office Block, Hotel Equatorial Shanghai  
No.65, Yan An Road (West), Shanghai, 200040, China  
中国上海市延安西路65号上海国际贵都大饭店办公楼405单元  
Phone: +86-21-62489820  
Fax: +86-21-62489821

© 2012 The Author(s). Licensee IntechOpen. This is an open access article distributed under the terms of the [Creative Commons Attribution 3.0 License](#), which permits unrestricted use, distribution, and reproduction in any medium, provided the original work is properly cited.